AEROMECHANICS OF THE ACTIVE ELEVON ROTOR

Mark V. Fulton
Research Scientist

Aeromechanics Branch
Aeroflightdynamics Directorate (AMRDEC)
US Army Research, Development, and Engineering Command
Ames Research Center, Moffett Field, California

The aeromechanics design of the Active Elevon Rotor (AER) has been completed. The AER elevon is a 15% chord, plain, trailing-edge flap actuated by a piezoceramic-based conformal actuator. A trade study is performed to determine the location of the elevon for reducing the (4/rev) vibratory hub loads at $\mu = 0.125$. Both single- and dual-elevon configurations are considered, with the dual-elevon configuration being selected. In addition, a linear engineering analysis is used to approximate elevon finite-span effects, which are found to be of sufficient size to warrant further investigation. Additional results are given for the selected AER design, including rotor blade modal frequencies and damping, and vibratory hub loads and elevon motions at four advance ratios. The design choice is predicted to have the six vibratory hub loads reduced by 50-90% at $\mu = 0.125$ and by 80-98% at $\mu = 0.225$; the effectiveness is compromised, however, at $\mu = 0.400$, with an 80% reduction of the vertical force being achieved at the expense of four other hub loads. Overall, the AER design should provide a reasonable basis for ongoing rotor blade development and future wind-tunnel testing.

Introduction

A project is underway to develop and test the Active Elevon Rotor (AER). The AER will have two independently actuated elevons (trailing-edge flaps) on each blade. Each elevon/actuator assembly uses Conformal Actuator Technology (CAT) developed by Domzalski Machine. This is a joint project of the US Army Aeroflightdynamics Directorate and the NASA Vehicle Systems Program.

Initial aeromechanics design work was documented in Ref. 1, which studied vibratory hub loads reduction and used linear sensitivity matrices calculated by CAMRAD II (Ref. 2). That initial approach used the flap and chord stiffnesses, and running mass, of an ideally-scaled 27% Apache (Ref. 3), augmented by estimated actuator weight; furthermore, Ref. 1 studied the effect of reduced torsion stiffness and a large array of Single-Wide (0.04 R) elevon radial positions.

The present work expands upon Ref. 1 by adding new elevon configurations and using the Regulator controls capability of CAMRAD II. The aeromechanics design process, and associated aeromechanics pre-test calculation results, will be described in this paper. The rationale for the selected elevon configuration will be given.

Planned wind tunnel testing will focus on vibratory hub loads reduction, but will also quantify (and reduce) vibratory blade loads, rotor power, and Blade Vortex Interaction (BVI) noise.

Design and Analysis Considerations

Physical Description

For this design study, the rotor blade is modeled to have one or two elevons. Each elevon is a 15% chord, plain, trailing-edge flap (Fig. 1). Two configuration types are modeled, a QW and a 2-DW; throughout, QW means "Quad-Wide" -- an elevon with a span of 0.16R; and 2-DW means "two Double-Wide" -- two elevons, each with a span of 0.08R.

The rotor has a hover tip Mach number of 0.65, a radius (R) of 6.48 feet, and a blade chord of 5.67 inches; in these respects, the rotor is identical to an ideally scaled 27% Apache. The planform is rectangular and the blade has a linear twist rate (of -10 deg/R) outboard of the root cutout. A single airfoil is used for the entire blade length -- a VR-18 with a 4% chord, -3 deg trailing-edge tab. The planform of the AER 2-DW design is depicted in Fig. 2, and general rotor characteristics are listed in Table 1.

The uniform passive blade structural properties, other than torsion stiffness, are taken from the ideally scaled 27% Apache properties (Ref. 3) and are listed in Table 2. The torsion stiffness in Table 2 is the value required to produce a first torsion natural frequency of 3.3/rev, the design target (explained later). The structural design concept (developed by Advanced Technologies, Inc.) will likely yield nearly uniform structural properties along the length of the blade, with an appreciable mass (and pitching inertia)

increment in each active section because of the presence of the actuator.

Each elevon will be part of a Conformal Actuator and Elevon Assembly (CAEA), based on technology developed by Domzalski Machine via an Army SBIR (DAAH10-99-C-0022) and described briefly in Ref. 4. The lower surface of the CAEA is flush with the lower surface of the blade, with the CAEA bonded in a recess in the blade structure; thus, the lower surface airfoil profile is uniform along the entire length of the blade, except for a small gap at the elevon edges -- the remaining CAEA/blade joints will be filled and faired. The upper surface airfoil profile is uniform, except for elevon edges and the upper surface interface between the elevon and the main airfoil (Fig. 1), which has a small gap to allow unimpeded motion of the elevon. (Flow through the gap on the leading-edge of the elevon will not occur, since the actuator blocks the flow.)

The CAEA uses a piezoceramic material for actuation and is sized to provide ±5 deg deflection of the elevon at 463 lb/ft^2, the dynamic pressure at 0.86R in hover. CAEA weight is modeled as 0.30 lb for a DW (0.08R) elevon, and 0.61 lb for a QW (0.16R) elevon, including additional balance weights to maintain the chordwise center of gravity. CAEA moment of inertia is 1.2E-4 and 2.5E-4 slug-ft^2 for a DW or QW elevon, respectively. Both the mass and inertia are uniformly distributed over the radial stations spanned by the elevon, and are added to the passive blade properties previously listed in Table 2. Note that a 0.61 lb, QW, balanced CAEA increases blade weight by about 20%.

As an elevon is moved further outboard, its peak motion limit, $|\delta|_{max}$, is decreased because the increasing dynamic pressure reduces the achievable deflection, given that the actuator can produce only a fixed amount of work. In particular, $|\delta|_{max} = 10$ deg/$(1+(r_\delta/0.86R)^2)$. For example, $|\delta|_{max} = 6.43$ deg for $r_\delta = 0.64R$; and $|\delta|_{max} = 4.77$ deg for $r_\delta = 0.90R$.

Comprehensive Analysis Model

All calculations were performed using a common structural model. This model consisted of eleven (11) structural elements for the blade, and several elements defining the articulating portions of the hub, with all parts of the hub being rigid. A rigid swashplate model was used with a pitch link modeled by a linear spring element. The fuselage was not modeled.

The aerodynamic surface of the blade was modeled as a lifting line with twenty (20) aerodynamic panels. The blade aerodynamic loads were calculated using table look-up to account for static nonlinearities due to angle of attack and Mach number. The airfoil table was developed by Boeing for a variant of the VR-12 similar to the airfoil contour being used for the AER, with CAMRAD II adjustment for zero-lift angle and a moment coefficient increment to account for a tab angle change. Dynamic stall was neglected. Unsteady aerodynamics was represented by the incompressible thin airfoil model.

The elevon was modeled as a prescribed aerodynamic flap with linear aerodynamic coefficients, $c_{l\delta} = 2.29$/rad and $c_{m\delta} = -0.427$/rad. These aerodynamic values are believed to be a good linearized choice from the nonlinear results given in Ref. 5. CAMRAD II calculations have not included any corrections for elevon end losses due to finite-span effects, although this issue is addressed via post-processing for a few data points.

A free wake model was used. Trim solutions included four iterations of the free wake, with a relaxation factor of 0.6. Subsequent Regulator solutions were initialized from the Trim solution, with the trim controls and the wake "frozen", i.e. with the wake geometry and influence coefficients fixed at their Trim values.

The Design Study, which investigated various radial positions for the elevon, was conduced with identical structural definitions, except that the location of the incremental mass/inertia of the CAEA(s) was moved to remain (radially) co-located with the elevon(s). The aerodynamic panel definitions were almost invariant with respect to the elevon placement, except when a QW (0.16R) elevon was placed at either 0.50R or 0.55R, in which case one panel edge was moved by up to 0.016R to coincide with the elevon edge. Thus, to a very large measure, the structural and aerodynamic discretization of the blade remained unchanged throughout the design study, with the dominant change being the location of the CAEA(s). Such results were mainly achieved by prearranging the number and location of the aerodynamic panels so as to accommodate a large assortment of DW elevon positions.

The lag damper (viscous damping and stiffness) and the pitch link (stiffness) were modeled with preliminary values for the Design Study and Elevon Finite-Span Effects, but more accurate values were used for the remaining calculations, as detailed in Table 3. These changes are believed to have had a negligible effect on the design trends, but may well change the magnitudes by a small amount. In particular, the lag damper change seems to have altered the uncontrolled vibratory hub loads index by about 5%, and the pitch link stiffness change affected the first torsion frequency by less than 0.02/rev.

Numerical Solution Methodology

Trim, Regulator, and Stability calculations were performed using CAMRAD II (Ref. 2), version 4.2.

Modal solutions were used for both Trim and Regulator solutions. Modal damping was 0.5% critical for the first eight (8) modes (i.e. through about 10/rev), except for $\mu = 0.400$, which used 1.0% critical for improved convergence.

Trim targets were a blade loading (C_T/σ) of 0.08 (thrust = 1,227 lb), a propulsive force of 2.0 ft^2 times the dynamic pressure, and zero 1/rev flapping; trim controls were collective, shaft tilt, and cyclic pitch angles. The (model scale) fuselage equivalent flat plate

area of 2.0 ft^2 is 0.015 times the rotor area and yields –5.7 deg shaft tilt for the baseline model at an advance ratio of 0.30.

Elevon effectiveness was inferred by calculating both the uncontrolled and controlled vibratory hub loads. The uncontrolled response has zero elevon motion; the controlled response has 3/rev, 4/rev, and 5/rev harmonic motions of each elevon adjusted by the Regulator, such that a regulator performance index (f) is minimized. The regulator performance index is a combination of a vibratory hub loads index and a control penalty for each of the elevons. The hub loads consist of three forces (longitudinal: F_X, lateral: F_Y, and vertical: F_Z) and three moments (roll: M_X, pitch: M_Y, and yaw: M_Z). The regulator performance index (f) includes the 4/rev sine and cosine harmonics of all six hub loads, plus weighted harmonics of the control deflections:

$$f = \left(\tfrac{1}{2}\right)\sqrt{F_{X4}^2 + F_{Y4}^2 + F_{Z4}^2 + M_{X4}^2 + M_{Y4}^2 + M_{Z4}^2 + \sum_{i=3}^{5}\left(W_{IB}\delta_{IBi}^2 + W_{OB}\delta_{OBi}^2\right)}$$

where

$$F_{*4}^2 = F_{*c4}^2 + F_{*s4}^2$$

$$\delta_{IBi}^2 = \delta_{IBci}^2 + \delta_{IBsi}^2$$

$$\delta_{OBi}^2 = \delta_{OBci}^2 + \delta_{OBsi}^2$$

If the QW configuration is involved, however, $\delta_{OB} = 0$ and δ_{IB} is replaced by δ_{QW}. The vibratory hub loads index (or "vibration index") is merely f above with the control values (δ_{IB} and δ_{OB}) omitted. Here, ( )$_{ci}$ and ( )$_{si}$ are the cosine and sine components, respectively, of the i/rev magnitude, where i is 4 for the hub loads, and 3, 4, or 5 for the elevon deflections. When the equation for f is expanded by substitution of the subsequent definitions, there are 12 hub loads terms plus 6 controls terms for each elevon. In this paper, all 12 hub loads terms have a weighting of 1.0, and the controls terms are multiplied by one weighting for each elevon.

Regulator solutions were implemented using a T-matrix approach, where the T-matrix is calculated once using a central differencing scheme with a control step of 1.0 deg. A relaxation factor of 0.2 was used, and 30 Regulator iterations were found to provide good convergence. The control penalty weightings (W_{IB} and W_{OB}) were manually set before each Regulator solution; iteration was used until the peak elevon deflection at the end of the Regulator solution was within 2% of its limit. For the design study (Fig. 5 and Table 4), a post-processing linear method was used to slightly reduce the elevon effectiveness for cases that had elevon motion in excess of the elevon limit; for all other presented cases, this procedure was not used, as the change is minor, and the interrelatedness of the different results (elevon deflection, vibratory hub loads, etc.) needed to be maintained.

Dynamics Considerations

Stiffnesses and Frequencies

The specification of blade stiffnesses was guided by a combination of engineering judgment and limited numerical analysis. To a large degree, there was a desire that the rotor have "representative" dynamics and sufficient strength for "representative" wind tunnel testing, up to an advance ratio (μ) of 0.35, for a blade loading of $C_T/\sigma = 0.08$. Nonetheless, it was also desirable that the rotor structure be tailored for enhanced elevon effectiveness, especially for the reduction of (4/rev) vibratory hub loads. Consequently, the flap and chord stiffnesses were taken from an ideally-scaled 27% Apache (Ref. 3), but the torsion stiffness was reduced (Ref. 1).

Initial calculations (Ref. 1) were performed for a large assortment of Single-Wide (0.04R) elevon radial positions; those calculations showed that the optimal first torsion frequency ($\omega_{\phi1}$) was 3.3/rev. More recent calculations for a nominal QW (r_{QW}=0.64R, μ = 0.125), demonstrated the optimum to be $\omega_{\phi1}$=3.7/rev, with 3.3/rev being nearly as good. Based on these two initial studies, $\omega_{\phi1}$=3.3/rev was selected as being "near optimal" and "more interesting" from a blade deformation perspective.

The resulting AER rotor blade is soft in-plane ($\omega_{\zeta1}$ = 0.26/rev) and has representative flap dynamics, with modal frequencies of $\omega_{\beta1}$=1.03/rev and $\omega_{\beta2}$=2.7/rev (Fig. 3); furthermore, the first torsion frequency is $\omega_{\phi1}$=3.3/rev. The blade detail design results indicate that the frequency will be no higher than $\omega_{\phi1}$=3.7/rev and the blade will have adequate torsion strength. The frequencies in Fig. 3 are for operation in a vacuum, with the rotor blade mode set determined from linearized equations that neglect all damping terms.

Aeroelastic Stability

The isolated rotor blade eigenvalues (λ), for operation under Sea Level Standard atmospheric conditions, are presented in Fig. 4 for the AER 2-DW design. Here, the Real and Imaginary (Imag) parts of the eigenvalues are plotted as a function of rotor speed, up to 1.14 Ω_o. The damping of nearly all modes increases with rotor speed up to about 1.065 Ω_o, after which the flap modes and the fundamental lag mode begin to lose damping. The lag mode damping ratio drops to 1.8% critical by 1.14 Ω_o. (The damping ratio = damping/(critical damping) = –Real(λ)/|λ|.) An exception to these trends is found in the second lag mode, which has damping that is independent of rotor speed, up through 0.98 Ω_o, but then begins to increase; another exception is the fundamental torsion mode, which shows damping that always increases with rotor speed.

A check of the forward flight stability (up to μ = 0.400) shows a more complex behavior, with a minimum fundamental lag mode damping of 2.8% critical (at μ = 0.225). Future calculations will use the

Floquet solution to account for the effects of periodic coefficients. Furthermore, nonlinear lag damper effects could be modeled to account for reduced damping of the regressing lag mode in the presence of 1/rev lag motion; this effect alone, though, is not expected to make the regressing lag mode unstable, since the lag damper provides only about 1.5% critical damping. Finally, the assumed 0.5% modal structural damping is believed to be somewhat conservative (i.e. low), especially due to the presence of real flap and lag hinges. In brief, no aeroelastic instabilities have been found, for a range of rotor speeds (to 1.14 Ω_o) and advance ratios (to $\mu = 0.400$).

Ground resonance stability has been investigated through the use of the Deutsch criterion (Ref. 6). These calculations show the importance of low stand and rotor lag damping. The stand/tunnel mounting is being designed to keep the fundamental stand modes above the rotor regressing lag mode. The installed stand frequencies and damping will be measured to ensure that ground resonance is avoided.

Design Study

Since the initial calculations of Ref. 1 were completed, work has been performed to determine the optimal radial position of a QW (0.16R) elevon. In addition, a 2-DW (2 x 0.08R) configuration has also been considered. Both new configurations will be discussed here, with an emphasis on radial position of the elevon(s), and a relative comparison of the configurations. Vibratory hub loads reduction was calculated for the nominal rotor speed of $\Omega_o = 1070$ RPM and a blade loading (C_T/σ) of 0.08. Design work focused on transition flight at $\mu = 0.125$.

Figure 5 shows the (4/rev) vibratory hub loads index for both configurations (QW and 2-DW), as affected by the average radial position of the elevon mid-span(s), r_δ. The upper curves depict the uncontrolled responses (i.e. for zero elevon motion), and the lower curves show the controlled responses (i.e. with maximum allowable elevon motion for each data point). The two dashed curves, that begin at $r_\delta = 0.50R$ and end at $r_\delta = 0.92R$, are for the QW configuration. The remaining curves are for three different 2-DW cases, with each case having a different location for the outboard (OB) elevon ($r_{OB} = 0.84$, 0.88, or 0.92R). For each 2-DW case, the inboard (IB) elevon location is varied to give different (average) r_δ. Note that, for the three 2-DW cases, the minimum r_δ is 0.70R, and occurs for the $r_{OB} = 0.84R$ case; and the maximum r_δ is 0.86R, for $r_{OB} = 0.92R$. Also, note that some of the r_{IB} values (namely 0.56, 0.64, 0.72, and 0.80R) are indicated below the controlled response curves; the identification of these r_{IB} values with the 2-DW cases (especially $r_{OB} = 0.88$ and 0.84R) is indicated by the nearly vertical fine-dashed lines, both for the controlled and the uncontrolled responses.

So, there are a total of four cases depicted, one for the QW configuration, plus three for the 2-DW configuration. Each of the four cases shows a controlled response that is substantially reduced from its corresponding uncontrolled response.

Uncontrolled Vibration Index

Perhaps the most amazing result is seen in the uncontrolled responses -- the elevon position has a significant effect for each case, even though there is no elevon motion. For example, the QW uncontrolled response peaks at 120 for $r_{QW} = 0.76R$, but is only 85 for $r_{QW} = 0.55R$, and 63 for $r_{QW} = 0.92R$. Similar variations are also seen in the 2-DW cases. The cause is clear -- the changed mass distribution significantly affects the vibratory hub loads index. This basic concept is not new, however, as structural tuning masses have been employed on rotor blades for decades.

There is also significant variation between one case and the next. In particular, comparing the different 2-DW cases, note that placing the OB elevon further outboard reduces the uncontrolled vibration index, with a minimum response predicted for $r_{OB} = 0.92R$ with $r_{IB} = 0.56R$ (or average $r_\delta = 0.74$). The QW configuration produces an even lower uncontrolled vibration index, but only for an elevon quite far outboard, $r_{QW} = 0.92$.

Controlled Vibration Index

Now consider the lower curves in Fig. 5, wherein the elevon harmonics are adjusted by the Regulator to minimize (or "control") the vibratory hub loads index. The curves for the controlled vibration index reveal the $r_{OB} = 0.92$ case to be an impressive performer, with a relatively flat index for IB elevon locations between 0.64 and 0.80R, inclusive. For all three 2-DW cases, $r_{IB} = 0.64R$ is the optimal choice -- it minimizes the controlled index and has an uncontrolled index that is moderate, especially for $r_{OB} = 0.88$ and 0.92R. Although the QW configuration can achieve a slightly lower controlled index, it does so only for a somewhat large radial position, namely, $r_{QW} = 0.88R$.

For AER, the outboard (OB) elevon position was selected to be "as far outboard as possible" to maximize its effectiveness -- via tip control of low frequency modes and a high dynamic pressure -- without being "too close to the tip" -- that could complicate elevon performance due to the presence of three dimensional blade tip effects. Specifically, the AER 2-DW design choice has the outboard elevon mid-span at $r_{OB} = 0.90R$ (thus placing the outboard edge of this elevon at 0.94R); and the inboard elevon mid-span is at $r_{IB} = 0.64R$. Both the uncontrolled and controlled responses for the AER 2-DW design are indicated on Fig. 5 with a diamond, which show the 2-DW design choice to have a relatively low vibratory hub loads index when using maximum allowable control effort, but only a moderately high index when uncontrolled.

Elevon Finite-Span Effects

It would be good, though, to estimate the importance of elevon finite-span effects. This is of particular interest because a change from a single QW (0.16R) elevon to two DW (0.08R) elevons cuts the (individual) active section's aspect ratio in half (i.e. from 2.2 to 1.1), thus increasing the aerodynamic losses due to edge effects. To begin, an estimate of the aerodynamic correction factors is developed.

An aileron static lift correction factor is available from Ref. 7 for a plain, 0.25 chord aileron at a wing tip; the static lift correction factors are 0.25 and 0.43 for the DW and QW aspect ratios, respectively. Operation at higher frequencies, though, would increase these factors, thus lessening the significance of the finite span effect; for example, Ref. 8 provides data for a plain, 0.15 chord flap with an intermediate aspect ratio (1.7), at several different frequencies; this data indicates that the (equivalent) 4/rev lift correction factors would actually be 50% larger than the static factors; consequently, the 4/rev lift correction factors are assumed to be 0.38 and 0.64 for the DW and QW elevons, respectively. The correction factors for pitching moment are larger than those for the lift (Ref. 8); consequently, the 4/rev pitching moment correction factors are assumed to be 0.96 and 0.98 for the DW and QW elevons, respectively. Finally, for this simplified analysis, only one aerodynamic correction factor is used, which is taken to be the average of the lift and pitching moment values; thus, the 4/rev aerodynamic correction factor is assumed to be 0.67 and 0.81 for the DW and QW elevons, respectively.

Now, a linearized analysis of the finite span effect is conducted on four data points from Fig. 5, summarized and further analyzed in Table 4. The selection of these four data points can be understood by considering the following three details: 1) both the "Best QW" and "Best 2-DW" points are included, as judged (only) from the controlled vibratory hub loads index; 2) the "Best Inboard QW" result is included, which has the lowest QW controlled index for elevon positions inboard of 0.80R; and 3) the "AER 2-DW" design choice (r_{IB} = 0.64 and r_{OB} = 0.90R) is included.

Note that the first two data columns report the (uncorrected) index, both uncontrolled and controlled, identical to the values shown in Fig. 5; this shows that the Best QW and the Best 2-DW have a very similar (uncorrected) controlled index. The Delta column is merely the difference between the uncontrolled and controlled index columns -- it represents the effectiveness of the elevon(s) at *changing* the vibration index; this suggests that the 2-DW's are just slightly more effective than the QW's when finite-span effects are ignored. When the Delta (effectiveness) is multiplied by the aerodynamic correction factor (k), however, it becomes apparent that this small 2-DW aeroelastic advantage is more than eliminated; specifically, the Best QW has a corrected effectiveness (of Delta * k = 55) that is now 20% higher than the Best 2-DW (Delta * k = 46). Finally, when the Delta * k is

subtracted from the uncontrolled index, the "Controlled Index, Finite" is obtained; this shows that elevon end losses have caused the Best QW controlled index to double, whereas the Best 2-DW controlled index has tripled. These results suggest that, when finite-span effects express themselves, the Best QW might have a lower controlled index than the Best 2-DW. Although the linearized finite-span analysis performed here is rather crude, it shows a sufficiently large effect as to warrant further investigation.

Nonetheless, the AER design choice was for a 2-DW with r_{IB} = 0.64 and r_{OB} = 0.90R. This design is believed to have sufficient control authority for a good experimental investigation, and the presence of two elevons allows for increased experimental flexibility. In particular, the presence of two elevons allows the collection of two sets of transfer functions, so that the aeroelastic effectiveness of an inboard elevon can be directly compared with the effectiveness of an outboard elevon. Furthermore, dual-control is made possible, thus increasing the complexity and value of control algorithm investigations. In these respects, the 2-DW configuration provides for increased experimental test possibilities.

Advance Ratio Effects

Having studied the selection of the AER 2-DW design ($\omega_{\phi1}$=3.3/rev, r_{IB} = 0.64, r_{OB} = 0.90R), including its frequencies and damping, the vibratory hub loads and elevon deflections for this design will now be examined for a range of advance ratios (μ = 0.125, 0.225, 0.325, and 0.400). This check helps to ensure that the selected rotor behaves reasonably and can reduce the vibratory hub loads that are induced at high speed.

Vibratory Hub Loads: Index and Six Components

First, consider the variation of the (4/rev) vibratory hub loads index with advance ratio, both uncontrolled and controlled. Figure 6 shows that the uncontrolled index varies as expected, being large at transition speeds, dropping for cruise, then rising again at high speed. The controlled index follows a similar trend. For the four advance ratios checked, the controlled response is reduced by 65% (μ = 0.400) to 90% (μ = 0.225) relative to the corresponding uncontrolled index. Furthermore, the controlled index remains less than the uncontrolled index envelope; that is, even the maximum controlled index (μ = 0.400) is less than the minimum uncontrolled index (μ = 0.225). These results suggest that the AER 2-DW design should function well, even at high speed. It would be informative, though, to look at the response in more detail.

All six components of the vibratory hub loads are summarized in Fig. 7. This figure provides the 4/rev magnitude of each hub load component, for the four advance ratios, both uncontrolled and controlled. At μ = 0.125, the vertical force (4/rev magnitude) is 160 lb, or 13% of the steady thrust -- a believable result for an

isolated rotor. For this speed, all six components are reduced significantly -- by 50% (yaw moment) to 90% (vertical force). Recall that the (vibration index) weightings were identical for all six hub load components. (Different reductions could likely be achieved with different weightings, although the peak elevon deflection must remain constrained to a physically realizable value.)

An examination of the results for $\mu = 0.225$ reveals that, except for the pitching moment, the controlled hub loads are reduced to even lower levels (than for $\mu = 0.125$). In fact, the vertical force is essentially eliminated -- it is reduced to 0.7 lb, or 0.06% of the steady thrust. Furthermore, the six components are reduced by 80% (yaw moment) to 98% (vertical force).

Finally, consider the results for $\mu = 0.400$. Whereas the vibration index showed a reduction of 65% (Fig. 6), the itemized hub loads of Fig. 7 reveal that a compromise is being made -- although the two largest components (vertical and lateral forces) are reduced, the remaining four components (longitudinal force; roll, pitch, and yaw moments) are actually increased. So, although the vertical force is reduced by 80%, it is achieved at the expense of other components, especially the moments. One small comfort is that even the moments are "controlled" to levels less than their uncontrolled values at $\mu = 0.125$.

Elevon Deflections: Time Histories and Harmonics

Now, consider the composition of the elevon deflections, both as time (azimuthal) histories and in harmonic form. The most striking example of (seeming) cooperation between the two elevons is apparent in the time histories for $\mu = 0.125$ (Fig. 8) and $\mu = 0.325$ (Fig. 9); a comparison of Fig.'s 8 and 9 shows that the two elevons are behaving more similarly in transition than for the higher speed. Another discernable difference is that the peak deflection for the inboard elevon is larger than for the outboard elevon; this is not a choice the controller has made -- the control weightings were individually adjusted until each elevon was working to its limit.

A different way to compare the elevon deflections is to look at the individual harmonics. For completeness, both the magnitude and phase of the harmonics is presented in Fig.'s 10a and 10b, respectively, for all four advance ratios. Figure 10a provides further evidence for previous observations from the time histories. For instance, for $\mu = 0.125$, Fig. 10a clearly shows that there is strong 3/rev and 4/rev participation, with less 5/rev deflection, for both the inboard and outboard elevons; for $\mu = 0.325$, however, the inboard elevon has a larger 3/rev participation, particularly at the expense of its 4/rev deflection, whereas the outboard elevon has made a different adjustment by reducing its use of 3/rev and 4/rev, but increasing the 5/rev harmonic.

Concluding Remarks

The aeromechanics design of the Active Elevon Rotor (AER) has been completed. The elevon is a 15% chord, plain, trailing-edge flap actuated by a piezoceramic-based conformal actuator. The uniform blade stiffnesses are selected to match the 27% Apache for flap and chord, but the torsion stiffness is reduced to provide a first torsion natural frequency of 3.3/rev. This approach is expected to enhance the effectiveness of the elevon while retaining representative flap dynamics. The following summarizes the principal findings of this study:

1) The uncontrolled vibratory hub loads index is strongly affected by the radial position of the actuator/elevon assembly, both for the single-elevon (QW) and dual-elevon (2-DW) configurations.

2) An approximate, linear engineering analysis suggests that finite-span effects can reduce the effectiveness of short elevons enough to diminish or even reverse the aeroelastic advantages of the dual-elevon configuration. The aerodynamic correction factor, which is reduced from 0.81 to 0.67 when lowering the elevon span from 0.16R to 0.08R, is sufficiently important to warrant further investigation.

3) A dual-elevon (2 x 0.08R) configuration was selected for AER, largely for its increased experimental test possibilities. The outboard elevon mid-span was specified to be at $r_{OB} = 0.90R$ to keep this elevon largely removed from the complications of three dimensional flow at the blade tip. The inboard elevon was selected to be at $r_{IB} = 0.64R$ based on the design study, which showed this radial location to minimize the controlled vibration index for $\mu = 0.125$.

4) AER dynamics, including blade modal frequencies and damping, appear representative and suitable for experimental testing.

5) The six AER vibratory hub loads are predicted to be reduced by 50-90% at $\mu = 0.125$ and by 80-98% at $\mu = 0.225$; the effectiveness is compromised, however, at $\mu = 0.400$, with an 80% reduction of the vertical force being achieved at the expense of four other hub loads.

Overall, the selected AER design should provide a reasonable basis for ongoing rotor blade development and future wind-tunnel testing.

References

[1]Fulton, M.V., "Design of the Active Elevon Rotor for Low Vibration," American Helicopter Society Aeromechanics Specialists' Meeting, Atlanta, Georgia, November 2000.

[2]Johnson, W., "Technology Drivers in the Development of CAMRAD II," American Helicopter Society Aeromechanics Specialists' Conference, San Francisco, California, January 1994.

[3]Straub, F.K., and Johnston, R.A., "Aeroelasticity and Mechanical Stability Report, 0.27 Mach Scale Model of the YAH-64 Advanced Attack Helicopter," NASA CR 178284, May 1987.

[4]Domzalski Machine, "Deformable Trailing Edges and Smart Material Actuation for Active Control of Rotor Blades," Ninth International Workshop on Aeroelasticity in Rotorcraft Systems, University of Michigan, October 2001.

[5]Wong, R.L., "CFD-Based Prediction of Rotor Elevon Effectiveness," MS Thesis, University of California, Davis, 2002.

[6]Johnson, W., *Helicopter Theory*, Dover Publications, Inc., New York, 1994, p. 683.

[7]McCormick, B.W., *Aerodynamics, Aeronautics, and Flight Mechanics*, John Wiley & Sons, Inc., New York, 1995, p. 518.

[8]van der Wall, B.G., and Geißler, W., "Experimental and Numerical Investigations on Steady and Unsteady Behaviour of a Rotor Airfoil with a Piezoelectric Trailing Edge Flap," Proceedings of the 55th Annual Forum of the American Helicopter Society, Montréal, Canada, May 1999.
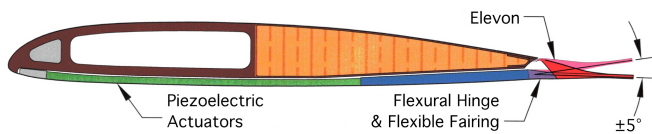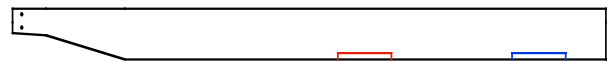
Fig. 1. Schematic of the active cross-section.

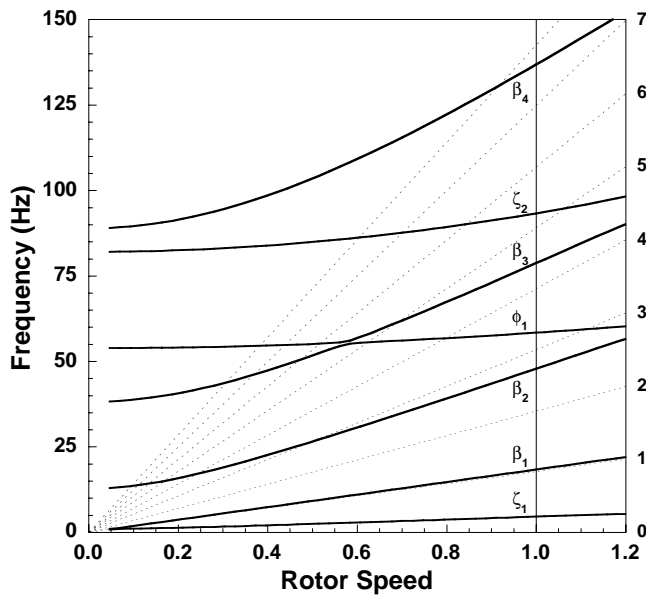**Fig. 2. Schematic of the AER 2-DW planform, with inboard (.64R) and outboard (.90R) elevons.**

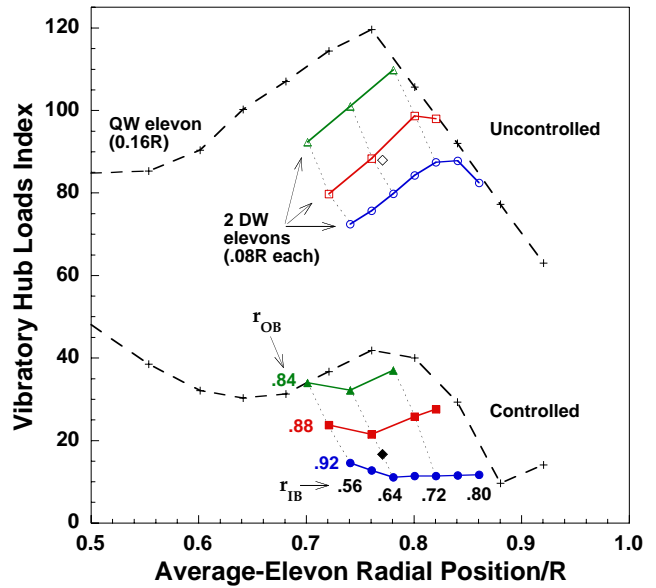Fig. 3. Fan plot of rotor blade frequencies in a vacuum, AER 2-DW, Ω_o = 1070 RPM, θ_o = 8°.

Fig. 5. Sensitivity of uncontrolled and controlled (4/rev) vibratory hub loads index to elevon radial position, both for QW (.16R) and 2-DW (2 x 0.08R) elevon configurations; IB=inboard, OB=outboard, diamond = AER 2-DW design choice.
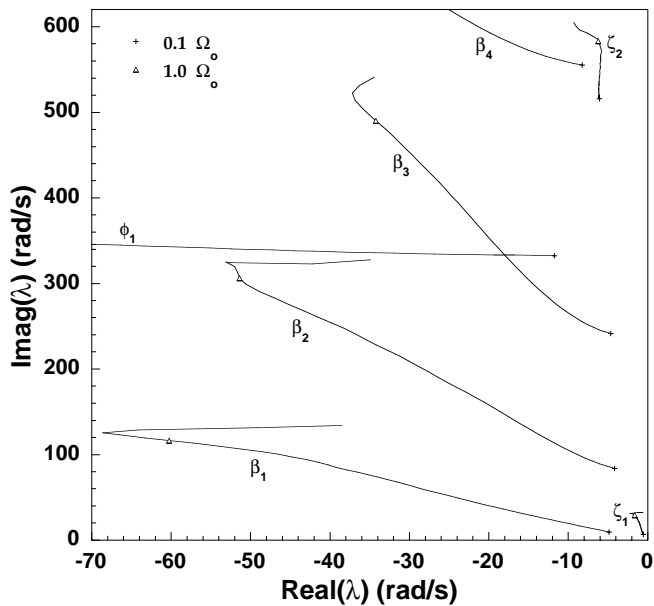

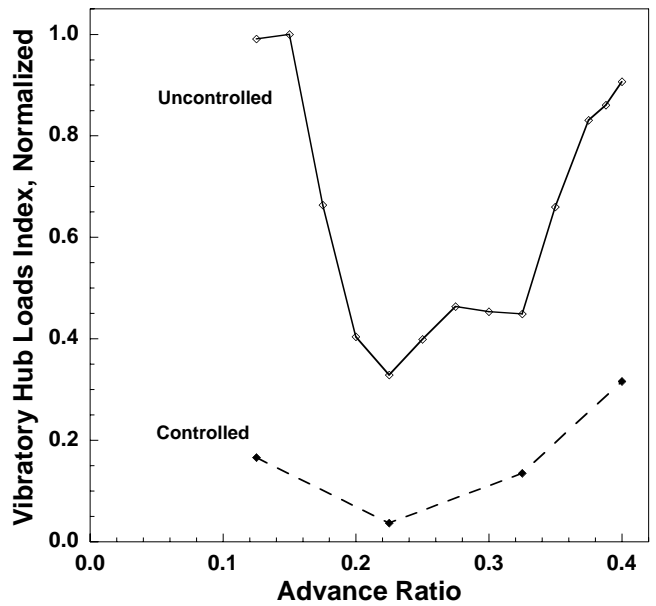Fig. 4. Effect of rotor speed on rotor blade eigenvalues (λ), AER 2-DW, Ω_o = 1070 RPM, θ_o = 8°.

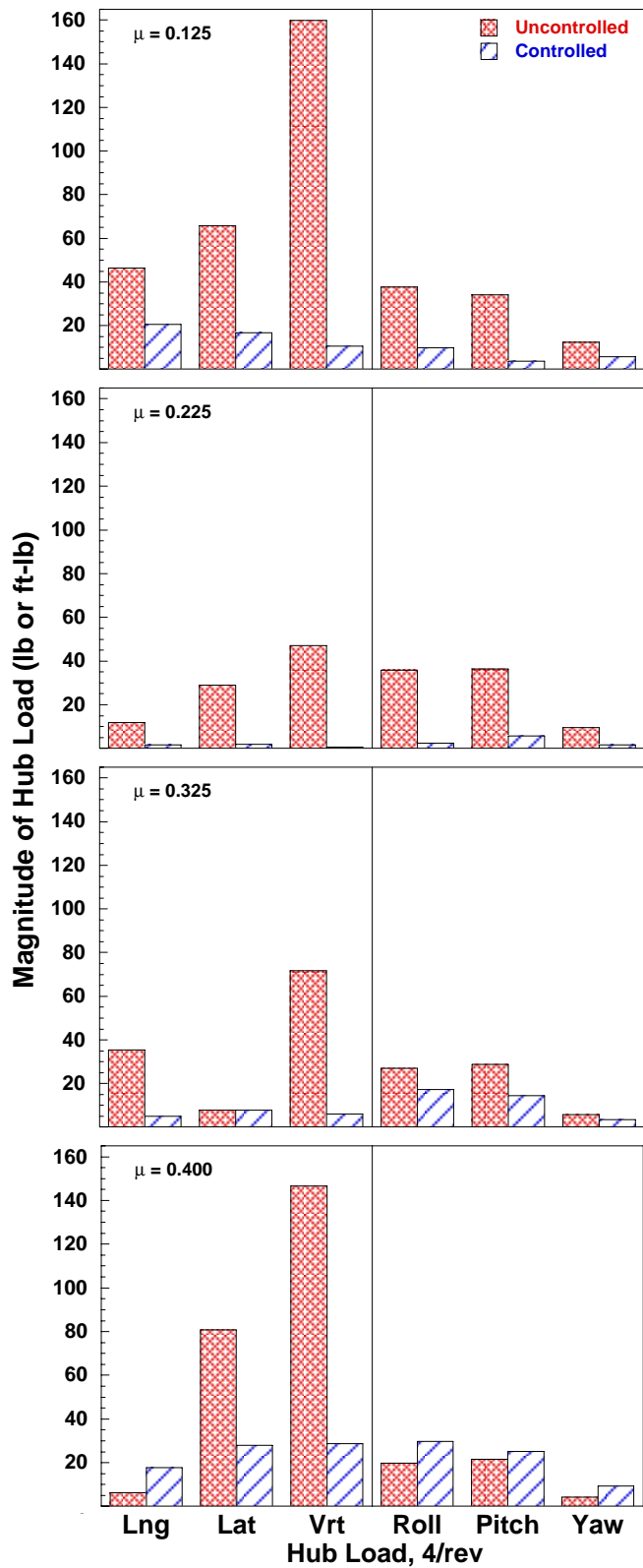Fig. 6. Elevon effectiveness for reducing the (4/rev) vibration index for a range of advance ratios.

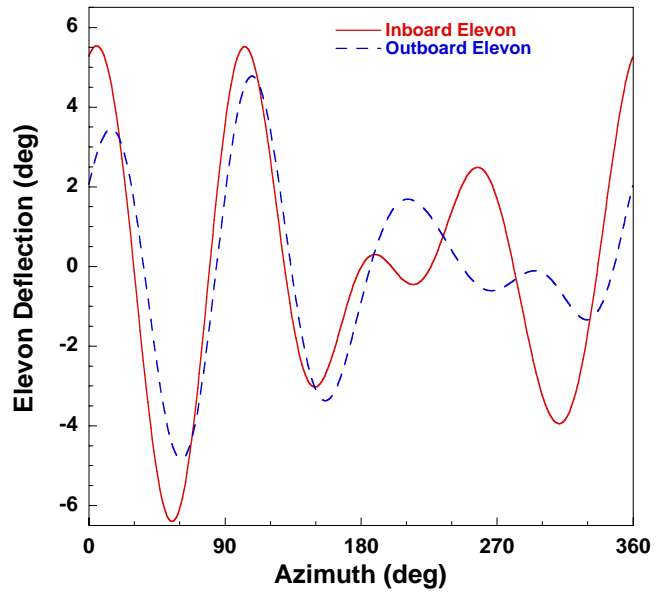Fig. 7. Elevon effectiveness for reducing 4/rev vibratory hub loads for four different advance ratios.
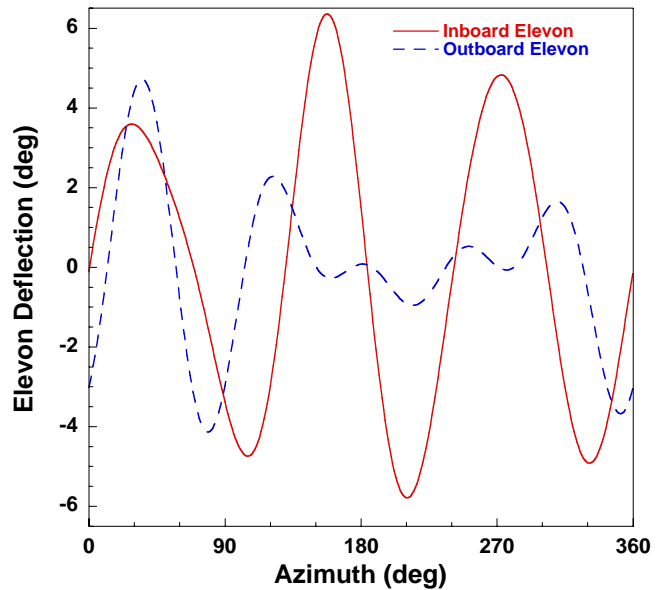

Fig. 8. Elevon deflection time histories, μ = 0.125.

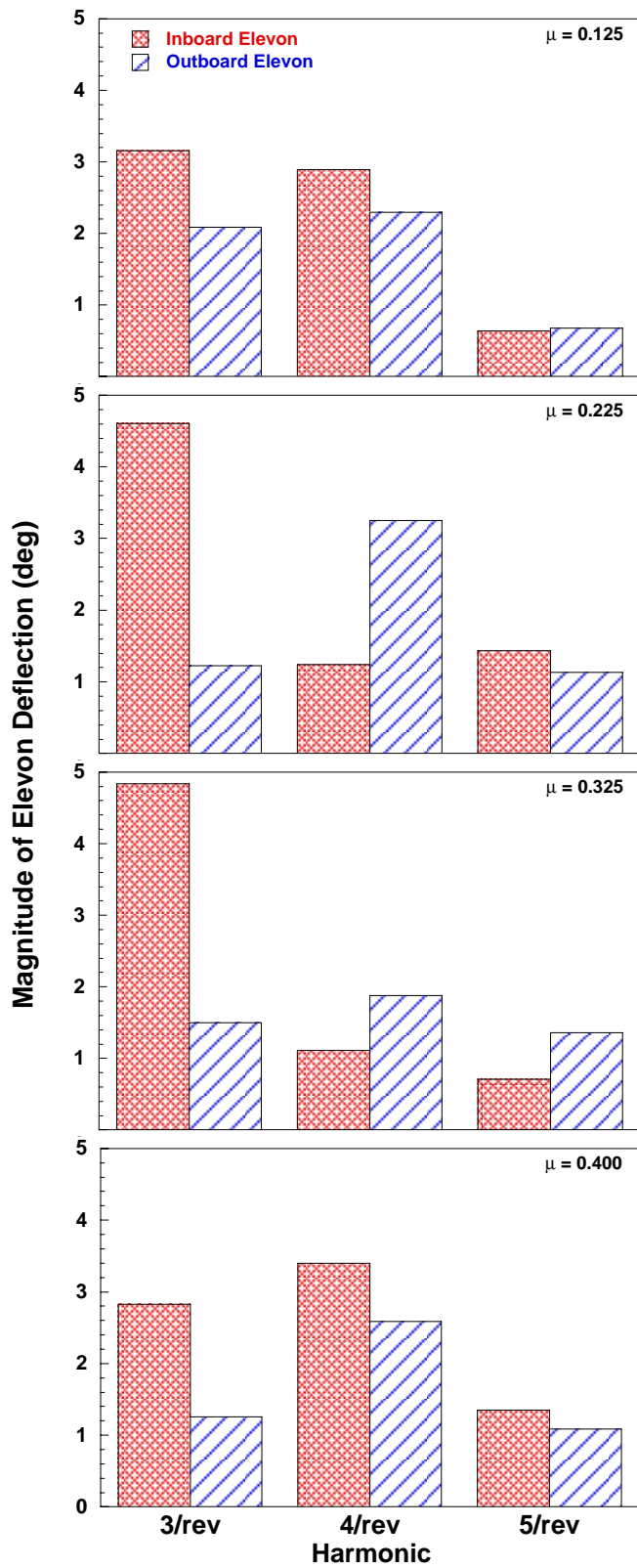Fig. 9. Elevon deflection time histories, μ = 0.325.

Fig. 10a. Magnitude of elevon deflection harmonics for both inboard and outboard elevons for four different advance ratios.
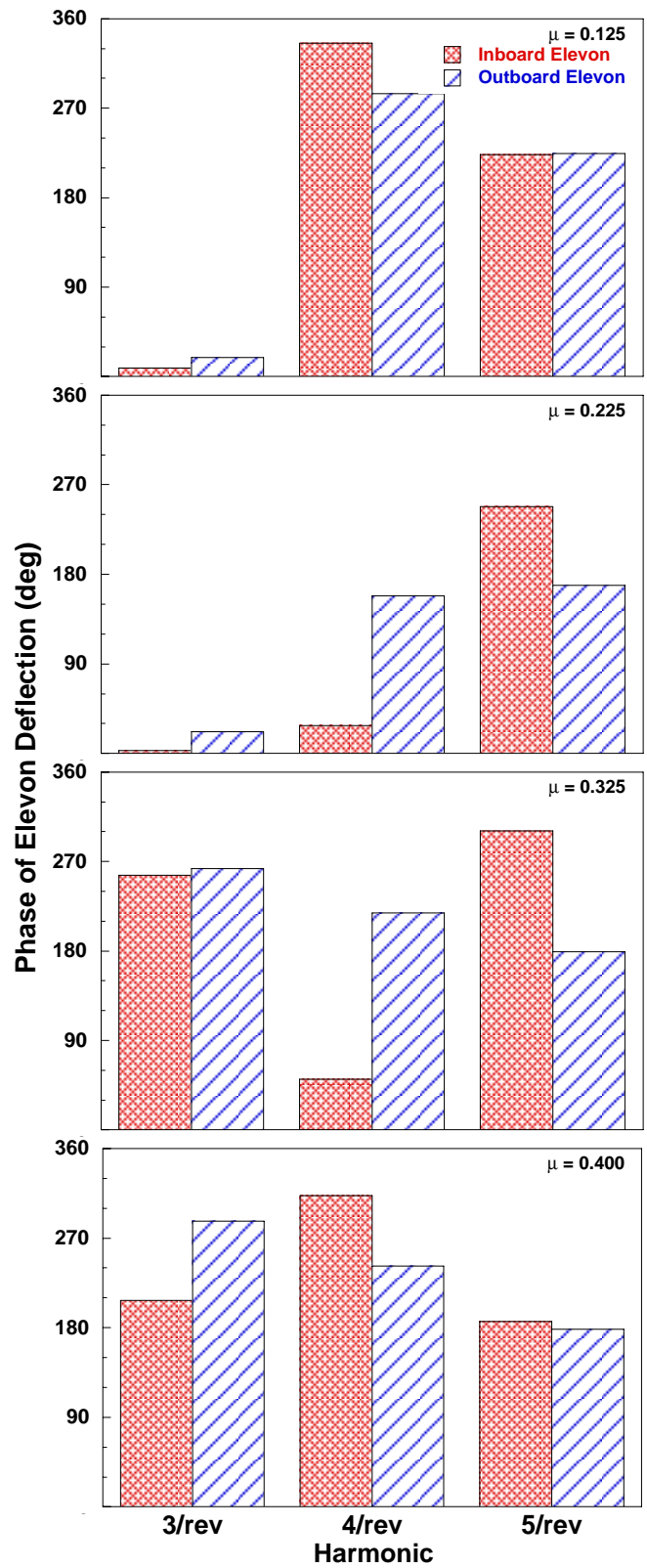
Fig. 10b. Phase of elevon deflection harmonics.

Table 1. General rotor characteristics.

Description	Variable	Value
No. of Blades	b	4
Rotor Radius, ft	R	6.48 (77.76 in)
Airfoil Chord, in	c	5.670
Solidity (bc/πR)	σ	0.0928
Twist, Linear, deg	θ_{pt}	-10
Feathering & Twist Axes		0.27c
Blade Elastic Axis		0.20c
Blade Center of Gravity		0.263c
Blade Tensile Axis		0.263c
Flap-Lag Hinge Location, in	e	2.97 (0.0382R)
Blade Grip Location, in	r_g	10.530 (0.1354R)
Root Cutout Location, in	r_c	22.17 (0.2851R)
Elevon Chord, Plain, in	c_δ	0.850 (0.15c)
Elevon Motion, deg	δ	±5.0 at $r_\delta = 0.86R$
Density, Air, slug/ft	ρ_0	0.002377
Nominal Rotor Speed, RPM	Ω_0	1070 (17.83 Hz)
Mach Number, hover	M_{tip}	0.6504

Table 2. Uniform passive blade section properties (r = 22.17 to 77.76 in), $\omega_{\phi1}$ = 3.3/rev.

Property	Value
EI_{Flap}, lb-in^2	1.095 E5
EI_{Chord}, lb-in^2	4.55 E6
GJ, lb-in^2	3.87 E4
m, lb/in	0.0368
I_θ, lb-in	0.0684

Table 3. Lag damper and pitch link characteristics.

Description	Variable	Design Study (Fig. 5 & Table 4)	Remaining Calculations
Lag Stiffness, ft-lb/rad	K_ζ	0	58.3
Lag Damping, ft-lb/(rad/s)	D_ζ	8.48	1.40
Pitch Link Stiffness, lb/ft	KPL	60.0 E5	4.01 E5

Table 4. The influence of elevon finite-span losses, where "Index" is the (4/rev) "Vibratory Hub Loads Index", Delta = Uncontrolled - Controlled, and k is the (4/rev) average finite-span aerodynamic correction factor.

	Uncontrolled Index	Controlled Index	Delta (Index)	k	Delta * k	Controlled Index, Finite
Best Inboard QW (.64)	100	30	70	.81	57	44
Best QW (.88)	77	9.6	68	.81	55	22
Best 2-DW (.64/.92)	80	11	69	.67	46	34
AER 2-DW (.64/.90)	88	17	71	.67	48	40